Nanosecond time-scale switching of permalloy thin film elements studied by wide-field time-resolved Kerr microscopy

Dmitry Chumakov, Jeffrey McCord,* Rudolf Schäfer,† and Ludwig Schultz
Leibniz Institute for Solid State and Materials Research IFW Dresden, Institute for Metallic Materials, Helmholtzstrasse 20, 01069 Dresden, Germany

Hartmut Vinzelberg, Rainer Kaltofen, and Ingolf Mönch
Leibniz Institute for Solid State and Materials Research IFW Dresden, Institute for Solid State Research, Helmholtzstrasse 20, 01069 Dresden, Germany

(Received 7 July 2004; revised manuscript received 5 October 2004; published 7 January 2005)

The switching of extended $Ni_{81}Fe_{19}$ thin film elements with a thickness of 50 nm and various shapes (squared, rectangular, pointed) has been studied by time-resolved stroboscopic Kerr microscopy based on a conventional wide-field optical polarization microscope. The elements are deposited on coplanar strip-lines that generate field pulses driven by electronic pulse generators. Time resolution is obtained by imaging with a gated and intensified charge-coupled device camera. The opening can be varied from 250 ps to continuous exposure, allowing the comparison of fast magnetization processes and quasistatic switching in slowly varying fields. The latter is typically characterized by the formation of a concertina domain pattern that irreversibly decays in a multidomain ground state by the abrupt motion of vortices and domain walls. After excitation with fast field pulses similar blocked patterns are formed. They dissolve by spatially inhomogeneous rotational processes involving cross-tie-wall-like domain boundaries.

DOI: 10.1103/PhysRevB.71.014410 PACS number(s): 75.60.−d, 75.70.−i

I. INTRODUCTION

Structured soft magnetic films have been of interest for research and application for many decades. Examples are thin film inductors and recording heads, magnetoresistive sensors based on the anisotropic or giant magnetoresistance effects, or magnetic random access memories (MRAM). In any case, the knowledge of the magnetization behavior of the elements is of crucial importance for the successful engineering of magnetic devices and memories. In general, the remagnetization process of structured magnetic films proceeds by the development and reorganization of complicated domain states for elements larger than the single domain size. These processes are fundamentally different for slowly varying magnetic fields (quasistatic switching) and for excitation in high-frequency fields or sharp field pulses (dynamic switching). Quasistatic remagnetization has been studied for many years. Depending on the field history and direction, the magnetization more or less instantaneously follows the applied field by the motion of domain walls and vortices, by rotational processes, or by the jumpy decay of blocked domain states (for a review of possible processes see Chap. 5.5.4 in Ref. 1). The processes of dynamic switching, which are not nearly as well known, are expected to be completely different due to effects that are related to electron spins, responsible for the magnetic moment. Consequently, the dynamic processes may not be seen as a simple switch of magnetization direction as the magnetization will not be able to instantaneously follow the magnetic field. To reach a new direction, it will have to spin about the field axis, performing a damped precessional motion.[2] It may therefore last a certain while before the magnetization relaxes to its new equilibrium distribution after fast field excitation.

In recent years the problems of fast magnetization switching in patterned films have been increasingly addressed by micromagnetic simulations (for examples see Refs. 2–4), which are reliably possible for elements in the submicrometer regime. Also experimentally there was progress, mainly based on magneto-optical techniques. These methods apply a stroboscopic principle: The initial magnetic state is disturbed by a train of short field pulses that are repeated periodically, allowing a sufficient interval between each pulse for the sample to return to the initial state. With a defined time delay relative to the field pulses the orientation of magnetization is then probed by measuring the magneto-optical signal, either integrally or spatially resolved, by summing up the signal of sufficient independent events to obtain a good signal-to-noise ratio. The latter, i.e., the dynamic imaging of fast magnetic switching, has a long history. Periodic magnetization processes were already imaged stroboscopically some 40 years ago, either by a pulsed light source[5,6] or by a gated video camera.[7] Time-resolved Kerr microscopy was applied to study the dynamical processes in electrical steel (e.g., Ref. 8), followed by observations in magnetic bubble films[9] and thin film recording heads.[10,11] Stimulated by the developments in the field of magnetoelectronics and novel MRAM concepts in recent years, dynamic imaging of magnetic film systems has gained renewed interest. The precessional motion in circular cobalt disks (diameter 6 μm, thickness 20 nm), excited by field pulses perpendicular to the film plane, was successfully imaged by Acremann *et al.*[12] by means of a time-resolved vectorial Kerr experiment with a 10 ps temporal resolution. Observations on permalloy thin film elements with in-plane field excitation were published by the Freeman group[13,14] (for a review see Ref. 15). They used a laser scanning Kerr microscope to stroboscopically image the switching of rectangular permalloy elements with a time resolution of 50 ps. The elements were deposited on gold transmission lines that created the field pulses. It was

shown that the switching time of an element can be strongly reduced from about 4 to 1 ns when the magnetization vector is pulsed by a longitudinal switching field while a steady transverse biasing field is applied, causing changes in the reversal mode. In a similar microscope Hiebert *et al.*[16] succeeded for the first time in the spatially resolved imaging of precessional switching,[2,17] i.e., switching in a magnetic field pulse that is applied orthogonal to the magnetization direction. Different modes of precession in the domains and walls of a pulse-field excited Landau pattern were found by Park *et al.*[18] in micron-sized permalloy elements, again by spatially resolved laser scanning Kerr microscopy. Besides magneto-optical Kerr microscopy, the new powerful imaging techniques based on x-ray magnetic circular dichroism (XMCD), which offer element-selectivity and a higher spatial resolution than Kerr microscopy, have been recently extended by stroboscopic imaging. The first time-resolved XMCD-based experiments using both x-ray photoemission electron microscopy[19–22] and x-ray microscopy[23] have been published.

For this paper we performed similar experiments as by the Freeman group. Instead of using a laser-scanning microscope, however, we implemented a stroboscope in a conventional wide-field Kerr microscope as it is otherwise routinely used for static and quasistatic imaging (most of the domain images in Ref. 1 have been obtained in such microscopes). Time resolution is achieved by imaging with a gated intensified charge-coupled device (CCD) camera. (Another wide-field setup, but based on a fixed repetition pulsed laser illumination source was developed in parallel and is published elsewhere.[24]) Our setup allows the simultaneous observation of the domain ground states together with their quasistatic switching properties under regular microscopical conditions, and the high-speed properties by using the stroboscopic mode. This is not achievable in the mentioned laser-scanning microscopes because there the magnetization is only probed at a small area with a focused laser beam by means of lock-in technique and it requires a certain amount of time to obtain a spatially resolved image by, e.g., scanning the sample under the microscope objective. The combination of dynamic and conventional imaging offers the possibility of a more detailed interpretation of the dynamic processes. The peculiarities of the high-speed magnetization processes can be readily identified, and in the static mode the domain ground states and influences of anisotropy are immediately obvious. For practical reasons we are restricted to the imaging of elements larger than a few micrometers, though the maximum spatial resolution of a typical wide-field Kerr microscope is around 0.3 μm based on the Raleigh criterion (this is also true for all other optical methods using visible light). Additional restrictions result from light scattering at the edges of patterned films that interfere with the image. Larger magnetic structures in the micrometer to 10 μm regime are nevertheless of interest from both a scientific and application point of view because they are used in recording heads, microinductors, and sensor applications. On the other hand it is well known that the domain ground states and quasistatic switching peculiarities of patterned low-anisotropy films remain similar in character for elements that vary in size over several orders of magnitude.[1] It is therefore expected that also the dynamic

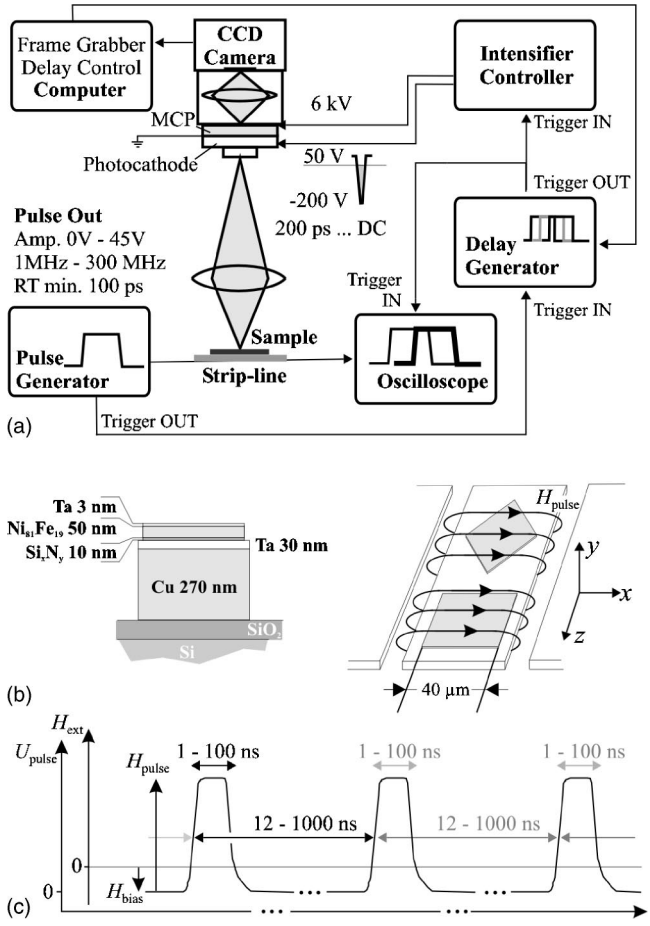

FIG. 1. (a) Scheme of the experimental setup for time-resolved domain imaging based on a gated CCD camera. (b) Sample, consisting of Cu micro strip-line, interlayers, and permalloy elements. (c) Train of field pulses with indications of the pulse duration and pulse separation possible in our stroboscopic experiments. The elements are excited by an effective magnetic field that is created by the superposition of pulse and external dc bias fields along the same axis.

features that are experimentally found in relatively large structures are also relevant for submicrometer elements, which are of interest in magnetic memories and which are readily accessible by micromagnetic simulations or by advanced imaging techniques like the mentioned XMCD methods.

II. EXPERIMENT

The experimental setup for stroboscopic domain imaging is schematically shown in Fig. 1(a). The main components are a wide-field polarization microscope (Zeiss JenaPol), equipped with a high-intensity xenon arc lamp and an intensified CCD camera from LaVision GmbH.[25] The photointensifier functions primarily as an electronic shutter. The incoming light hits the photocathode producing photoelectrons. The photocathode is permanently exposed to a positive potential of 50 V, which prevents the emitted electrons from leaving its surface. On the arrival of a trigger signal an im-

pulse of negative voltage (−200 V) is applied to the photocathode, pushing the photoelectrons into the microchannel plate (MCP) where they are accelerated and multiplied. After leaving the MCP the multiplied electrons are further accelerated before they finally hit the phosphor layer of the output window generating photons. The CCD camera accumulates these photons during integration time. One unique feature and advantage over existing laser based setups is that the effective opening time of the intensifier can be varied from 250 ps (corresponding to the maximum time resolution of our experiment) to continuous exposure. Furthermore, we are not restricted to a fixed-frequency illumination source in contrast to the before mentioned laser scanning technique. Therefore we are able to accumulate the images with frequencies ranging from dc up to 80 MHz, only limited by the image intensifier electronics. This gives us the opportunity to compare our time-resolved data directly to images acquired by static (dc) wide-field imaging. Also changes with different pulse repetition rates, e.g., related to long-term magnetic relaxation processes, can be studied. In connection with the variable gating time the experiment can be easily adapted to the used rf electronics and the experimental conditions needed for the particular magnetic system to be investigated. As no mechanical stepwise scanning is necessary in our case, the viewing field and the lateral resolution are determined by the microscope's optical parameters and the resolution of the camera system, limited by the MCP and the CCD resolution. The latter is close to the resolution of the microscope for the objective lens used in the presented experiments [100×, numerical aperture (NA)=0.9, spatial resolution=0.4 μm]. This correlation changes with lower magnification objectives, where the increase in viewing field scales disproportionately to the corresponding loss in resolution. The resolution limit is then determined by the parameters of the camera system. To improve the signal-to-noise ratio (SNR) for the low contrast imaging, the experiments presented here were done with 2×2 pixel binning on the CCD chip, thus reducing the actual lateral resolution to around 0.8 μm.

To achieve a reasonable SNR, the Kerr images of typically 10^6 independent events, excited by a train of field pulses that are repeated periodically, are integrated in time. The stroboscopic technique requires an accumulation over repeatable magnetization processes. From every acquired image an image of the saturated sample state, which is separately obtained by applying an external dc magnetic field, is digitally subtracted. As a result we obtain pictures that contain only magnetic information. By imaging identical processes with longitudinally and transversally aligned Kerr sensitivity, respectively, we are able to image the in-plane magnetization components separately at two orthogonal sensitivity directions of the Kerr contrast. In both cases, however, there is a contrast overlay of possible magnetization components perpendicular to the film plane. These can be imaged separately in the polar Kerr effect at perpendicular incidence (see Ref. 1 for details on the different Kerr effects).

The magnetic film elements to be imaged are deposited on top of a 50 Ω impedance-matched coplanar Cu waveguide [Fig. 1(b)]. Fast voltage pulses are sent through the center conductor of the strip-line to produce a rapidly changing magnetic in-plane field. A trigger signal synchronizes the image acquisition with the incoming pulse. An electronic delay line permits one to adjust the difference between trigger and pulse transition times. Thus, by changing the delay between pulse and image exposure, we are able to temporally probe the magnetization process. Details of the sample geometry are schematically shown in Fig. 1(b). The coplanar Cu strip-line with a thickness of 270 nm is deposited on a 600 μm thick Si/SiO_2 substrate. The 50 nm thick $Ni_{81}Fe_{19}$ elements are located on top of the central conductor and are covered with a 3 nm Ta cap layer to prevent oxidation. Before the magnetic elements are deposited, the stripe-line is covered by 30 nm Ta and 10 nm Si_3Ni_4. The Ta layer has optical reflection properties similar to those of the $Ni_{81}Fe_{19}$ film. This prevents the strip-line around the magnetic elements from strong and thus disturbing reflection, which would be the case for uncovered copper. The Si_3Ni_4 layer electrically insulates the strip-line. All depositions and patterning were done by sputtering and optical lithography, respectively. The width of the strip-line after etching is 41 μm, the width of the elements of various shapes is 40 μm, leaving 0.5 μm distance from the strip-line edges. The field values and distribution generated by the strip-lines were calculated analytically.

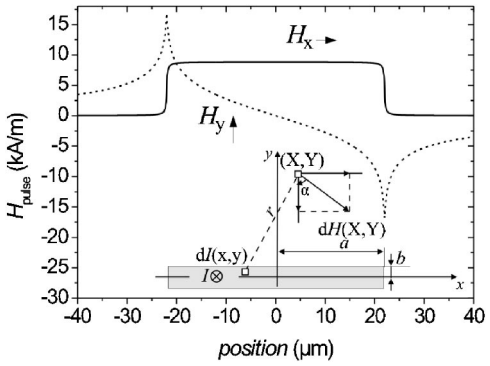

FIG. 2. Calculated field amplitudes perpendicular to the strip-line axis. H_x is the field parallel to the element, whereas H_y the field perpendicular to the element's plane.

For field analysis we assume that a small strip-line element with coordinates (x,y) and current density j produces at the point with the coordinates (X,Y) the following radial field:

$$dH(X,Y) = \frac{j \cdot dxdy}{2\pi \cdot r} = \frac{I \cdot dxdy}{8\pi \cdot ab \cdot \sqrt{(x-X)^2 + (y-Y)^2}}, \quad (1)$$

where I is the current, and a and b are the dimensions of the strip-line as indicated in the inset of Fig. 2. Considering $dH_x = dH \cdot \sin(\alpha)$ and integrating over the entire strip-line we obtain

$$H_x(X,Y) = \frac{-I}{8\pi \cdot ab} \int_{-a}^{a} \int_{-b}^{b} \frac{(y-Y)}{(x-X)^2 + (y-Y)^2} dydx \quad (2)$$

for the field aligned perpendicularly to the strip-line axis, i.e., longitudinally along the deposited film elements. A head-on integration brings us to analytical expressions for the longi-

tudinal field components. The first integration over x gives

$$H_x = \frac{-I}{8\pi ab}\left[\int_{-b}^{b} \arctan\left(\frac{u}{y-Y}\right)dy - \int_{-b}^{b} \arctan\left(\frac{v}{y-Y}\right)dy\right] \tag{3}$$

with $u=a-X$ and $v=-a-X$. Considering

$$\int \arctan\frac{1}{x}dx = x\arctan\frac{1}{x} + \frac{1}{2}\ln(x^2+1) \tag{4}$$

and substituting $g=b-Y$ and $h=-b-Y$ in the final expression, we derive

$$H_x = \frac{-I}{8\pi ab}\left[\begin{array}{l} u\left[\frac{1}{2}\ln\left(\frac{g^2+u^2}{h^2+u^2}\right) + \frac{g}{u}\arctan\left(\frac{u}{g}\right) - \frac{h}{u}\arctan\left(\frac{u}{h}\right)\right] \\ -v\left[\frac{1}{2}\ln\left(\frac{g^2+v^2}{v^2+h^2}\right) + \frac{g}{v}\arctan\left(\frac{v}{g}\right) - \frac{h}{v}\arctan\left(\frac{v}{h}\right)\right] \end{array}\right]. \tag{5}$$

A similar calculation yields the following expression for the out-of-plane field:

$$H_y = \frac{I}{8\pi ab}\left[\begin{array}{l} g\left[\frac{1}{2}\ln\left(\frac{g^2+u^2}{v^2+g^2}\right) + \frac{u}{g}\arctan\left(\frac{g}{u}\right) - \frac{v}{g}\arctan\left(\frac{g}{v}\right)\right] \\ -h\left[\frac{1}{2}\ln\left(\frac{u^2+h^2}{v^2+h^2}\right) + \frac{u}{h}\arctan\left(\frac{h}{u}\right) - \frac{v}{h}\arctan\left(\frac{h}{v}\right)\right] \end{array}\right]. \tag{6}$$

Figure 2 shows the calculated longitudinal and polar field components along the x axis on the surface of the conductor. In accordance to our experiments, the calculations are performed for a 300 nm thick and 41 μm wide center conductor. The longitudinal field component is rather homogeneous and decreases almost linearly with increasing distance from the conductor surface (not shown). On the edges of the strip-line a strong out-of-plane component is present. For our thin film structure the influence of the perpendicular field is only of minor importance, since the demagnetizing field along the y axis is quite strong and thus the effective permeability is rather weak.

The calculated field values were checked experimentally by domain observation. A zero field vortex ground state (Landau state) was first adjusted in the elements by ac demagnetization. An application of a dc strip-line field resulted in a displacement of the central vortex from its zero field state. Afterwards a magnetic field was applied by external coils, which compensated the strip-line field and thus drove the vortex back into its initial position. The applied compensation field is therefore a measurefor the strip-line field. This approach sets a direct correspondence between the strip-line current and the generated field. Both the calculated and experimental field values agree very well, the values lie within 7% in amplitude. For the 41 μm waveguide we obtain an amplitude of 0.21 kA/m per volt (determined experimentally).

The pulse amplitude, duration, risetime, and pulse distance can be varied as indicated in Fig. 1(c), depending on the pulse generator used. In this paper we present results obtained for 10 ns wide +39 V pulses (generating a field amplitude H_{pulse} of 8.3 kA/m that is also the maximum available field in our experimental setup) with a 20/80-risetime of 360 ps. Higher fields are possible in principle with the use of a strip-line of reduced width. The pulse separation was approximately 1000 ns, thus ensuring a static initial magnetization pattern at the onset of the pulse. The effective magnetic field acting on the sample is modified by a negative dc-field H_{bias} of variable amplitude that is externally applied opposite to the pulse field direction [Fig. 1(c)]. If, for instance, the sample is exposed to a bias field of $H_{bias}=-2$ kA/m, this results in an acting field H_{total} of +6.3 kA/m at the pulse presence and −2 kA/m during the pulse absence.

III. RESULTS AND DISCUSSION

Time-resolved imaging was applied to permalloy film elements, which were switched from positive to negative saturation by the superposition of pulse and bias fields. Rectangular elements of different aspect ratios, square elements with the field applied along the edge and diagonal, and elements with pointed shape were studied. In each case the quasistatic processes were investigated for comparison. All elements had a length of 40 μm along the field direction as already indicated in Fig. 1(b).

The results for square-shaped elements in diagonal magnetic fields are collected in Figs. 3–6. The processes of quasistatic switching are presented in Fig. 3. Here the images were recorded under non stroboscopic conditions with the magnetic field held constant during different steps of the reversal. Shown are several magnetization states at longitudinal and transverse Kerr sensitivity while a positive field is slowly reduced and inverted. Switching is characterized by the formation of a metastable van-den-Berg concertina

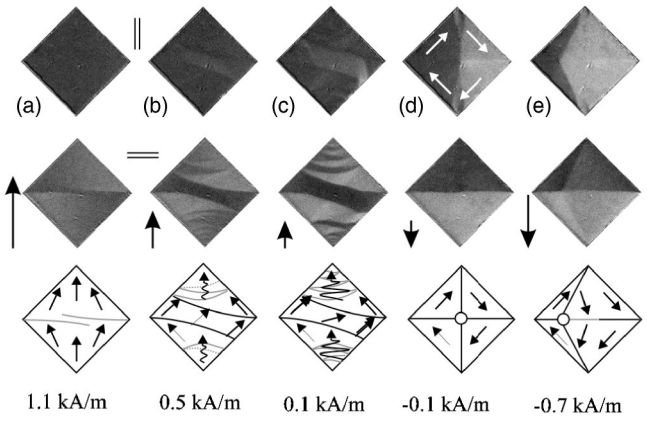

FIG. 3. Quasistatic magnetization process of a permalloy square (thickness 50 nm) in a slowly changing magnetic field applied along the diagonal axis as indicated. Similar states are shown with the Kerr sensitivity along (upper row) and transverse (lower row) to the field axis, together with a schematic drawing of the magnetization vector field as qualitatively derived from the Kerr contrast.

pattern[26] [(a)–(c)], also described as a blocked or "buckling" state.[1,27] The concertina becomes clearly visible at transverse sensitivity and is characterized by a system of interacting, low-angle Néel walls that stabilize themselves by dipolar fields.[1] It is formed by an alternating clock- and counterclockwise rotation of magnetization with a characteristic texture orthogonal to the average magnetization direction, caused by the stray field energy and based on the same mechanism as the formation of magnetization ripple.[28] Two main factors determine the development of the concertina pattern. First, the period itself is dominated by the effective width of the element. Similar to domains in patterned elements, where the domain width is determined by the wall energy and the anisotropy energy (see, e.g., Ref. 29), for smaller effective widths and thus in the corners of the tilted element narrow concertina patterns are favored. Interestingly, the orientation of the concertina walls reflects the contour lines of field penetration that occurs in stronger diagonal fields[30] (see Ref. 31 for further details on field penetration and hysteresis effects in similar elements). Experimentally, the concertina development is highly repeatable. Minor additional effects are due to the polycrystalline microstructure and possible edge defects of the patterned magnetic film. Note that the development of the concertinas is a highly hysteretic process and more than qualitative arguments cannot be given at this point. (A theoretical description of the concertina period with changing element dimensions exists.[32] However, so far the model is not confirmed by systematic experiments.) Around zero field the concertina breaks down abruptly by the formation or unpinning of Bloch lines at the edges, leaving the element in the four-domain Landau ground state [Fig. 3(d)]. In negative fields the domains magnetized favorably relative to the field direction grow by wall and center-vortex motion [Fig. 3(e)]. Note that the main switching event, i.e., the decay of the concertina [from Fig. 3(c) to Fig. 3(d)], is an irreproducible process that occurs at slightly different field values when the experiment is reproduced, thus leading to fluctuations in the switching field.

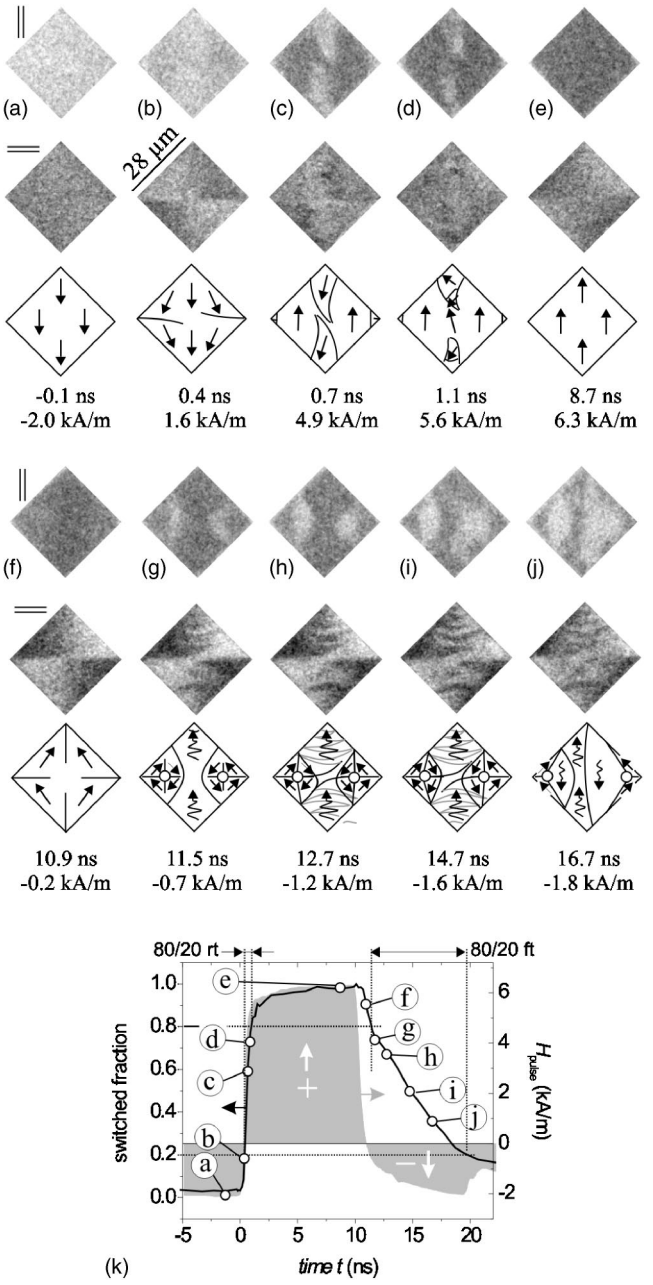

FIG. 4. (a)–(j) Time-resolved Kerr images at longitudinal and transverse sensitivity of the same element as shown in Fig. 3, but after excitation with a diagonally applied pulse field. Indicated is the effective field resulting from the superposition of a +8.3 kA/m pulse field and −2.0 kA/m dc field, and the time delay relative to the field pulse. The magnetization distribution at certain stages of the dynamic reversal is schematically indicated. (k) Plots of the longitudinal Kerr signal along the field axis as a function of time. A wave form of the exciting current pulse is overlaid in gray.

Figure 4 shows stroboscopically imaged Kerr pictures of the same element with pulse-field excitation along the diagonal direction, again observed at longitudinal and transverse Kerr sensitivities. In this experiment a bias field of −2.0 kA/m was superimposed on the +8.3 kA/m pulse field. The matching field pulse profile together with the averaged longitudinal Kerr signal is shown in Fig. 4(k). The series of

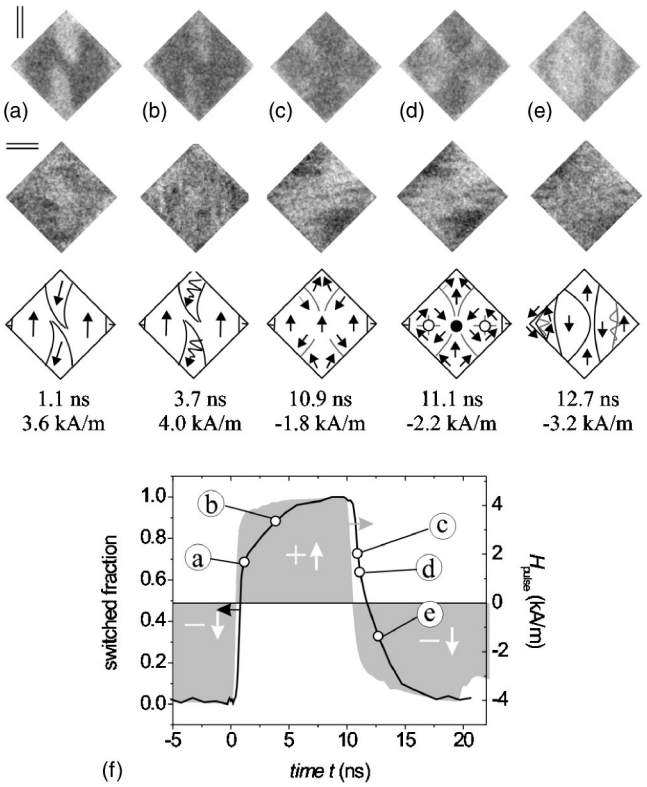

FIG. 5. (a)–(e) Time-resolved Kerr images of the square element as shown in Fig. 4, but with changed bias and thus changed excitation field. The effective field varies from −4.0 to +4.3 kA/m. (f) Plots of the longitudinal Kerr signal together with the pulse shape as a function of time.

pictures, which were obtained along the rising and falling edge of the field pulse, are assigned to the corresponding plot. The negative field amplitude is sufficient to saturate the samples as confirmed by hysteresis loop measurements of the elements. In the absence of the field pulse the element is kept saturated negatively by H_{bias}, as seen in the images of state (a) of Fig. 4. When the pulse field arrives, it results in a positive total field of 6.3 kA/m, forcing fast changes in the elements magnetization. Due to the local demagnetizing field, the switching process begins with magnetization rotation on the sides of the element as clearly seen in the transversal images, leaving the middle part of the element almost

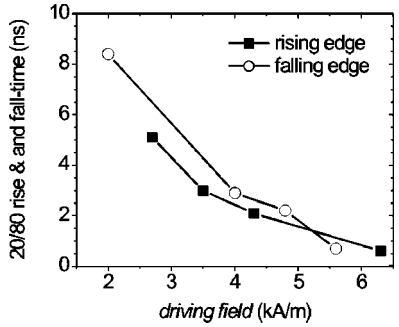

FIG. 6. Rise and, respectively, fall times (from 20% to 80% of signal amplitude) for different effective pulse field amplitudes derived from the longitudinal Kerr signal for the tilted element.

unchanged for a while. The central part is switching much slower, becomes narrower [Fig. 4(d)], and finally dissolves as the sample reaches positive saturation [Fig. 4(e)] after some nanoseconds. As indicated in the schematic vector plots, which were derived qualitatively from the Kerr images, the basic mechanism of remagnetization consists of inhomogeneous rotational processes that are determined by the initial rotational process, leading to head-on and tail-on magnetization structures along the center line of the element. Regions with stronger and weaker rotation appear as domain like areas in the longitudinal images [especially in Figs. 4(c) and 4(d)], which are separated by domain boundaries. Note that on the rising edge of the pulse the magnetization follows the field pulse instantaneously as evident from Fig. 4(k). This is not the case on the slower falling edge where a delay is measured. Here also the local magnetization processes [Figs. 4(f)–4(j)] differ from the reversal of the previous case. Again, the first changes of magnetization appear on the sides of the element in a symmetric way [Fig. 4(f)], but with lagging of switching not only the center region, but also the left and right corners of the element are prevented from strong rotations for some time [Figs. 4(g)–4(j)]. A detailed interpretation of the process as given in the schematic drawings is only possible by considering both longitudinal and transverse sensitivity images. In Fig. 4(f) the magnetization in the two side corners starts to rotate parallel to the edges as clearly visible in the transverse images. As discussed before, this is due to the shape anisotropy, favoring an alignment of magnetization parallel to the edges. With increasing amplitude of the opposing field a concertina pattern is formed by pure magnetization rotation in the center part [Fig. 4(g), transverse image] that is getting stronger in contrast [Figs. 4(h) and 4(i)], indicating an alternating and increasing clock- and counterclockwise rotation. The concertina strongly resembles that of the quasistatic case in Figs. 3(b) and 3(c). However, there is a significant difference that becomes obvious in the longitudinal images of Fig. 4. Whereas the concertina decays abruptly by domain wall motion in the quasistatic case, the magnetization continues to rotate in the negative direction (downwards in the images) by keeping its alternating character in the dynamic case. This change of magnetization is initiated symmetrically in the left and right halves of the element [at the vortex structures, Fig. 4(g)], forming brighter areas in the longitudinal images that expand with time [Figs. 4(h)–4(j)]. At the same time the rotation proceeds and the concertina vanishes continuously [Fig. 4(j), transverse image] until the initial state [Fig. 4(a)] is finally reached again after about 40 ns (not shown). Note that concertinas in rectangular elements have also been observed in the time-resolved studies of similar elements in Refs. 15 and 33.

One obvious difference in the behavior between the rising and falling edges of the pulse is the absence and presence, respectively, of a well-defined concertina pattern. In addition, vortex structures develop at the edges of the element along the falling edge. The "blocking" of magnetization, which is also the reason for the stability of concertinas in quasistatic switching, seems to play a similar role in the dynamic case. As a consequence, dynamic switching is slowed down once multidomain states (like concertinas) are involved which is more pronounced for the falling edge. The differences be-

tween domain nucleation at the rising and falling edges in our experiment can be explained by the effective opposing field amplitudes and the difference in switching speeds for the two pulse edges, respectively [Fig. 4(k)]. Note that the opposing negative field at the falling edge changes only slowly from 0 to −2 kA/m and reaches the maximum field amplitude only after 10 ns, resulting in a slow switching speed. An 80/20 rise time of 0.6 ns and a fall time of 8.5 ns is derived from the integrated magneto-optical signal. For the descending pulse, also a delay of switching relative to the occurrence of the reversing pulse field becomes visible. Before the field pulse is applied, the magnetization is forced downwards by a relatively low field of H_{total} −2 kA/m. A fast switching event, however, is then generated by the large opposing field of H_{total} = +6.3 kA/m. The magnetization reversal occurs almost instantaneously in the first step [Figs. 4(a)–4(c)]. Once the antiparallel aligned domains have developed, they are driven out by the large magnetic field. At the falling edge, on the other hand, the opposing field is rather weak and changes gradually over several nanoseconds. There is sufficient time for a domain network to be formed, consisting of the concertina and the mentioned vortices on the left and right sides of the element, thus involving multiple Bloch lines. The breakdown of the concertina by domain wall motion, however, is hindered in the case of dynamic switching due to the low mobility of the complicated wall and vortex structure. Slow relaxation processes due to low vortex mobility on the subnanosecond time scale have also been observed in Ref. 24, where the domain patterns were limited to simple magnetic ground states and the field excitation was restricted to low amplitude. Note that the vortex state itself has no net magnetization, leading to a zero effective magnetic torque and therefore strongly reduced mobility.[4] Concurrently with the occurrence of the multidomain state a kink in the magneto-optical response becomes apparent [at (g) in Fig. 4(k)]. (An interpretation of the vague domain boundary structure involved in the dynamic switching event will be given later in the paper.)

Following these arguments, we would expect a more symmetric behavior in the element switching by increasing the negative bias field. The reversal process from H_{ext} = −4 to 4.3 kA/m is shown in Fig. 5. Starting from the saturated state, the domains at the rising edge develop abruptly by magnetization rotation. Once the domains are generated the change of magnetization is rather slow due to the reduction of the effective field acting on the domains. This causes the pronounced kink [state (a)] in the magnetic response, seen in Fig. 5(f). Slow domain annihilation comparable to the falling edge of Figs. 4(g)–4(j) is observed along the rising edge of Figs. 5(a) and 5(b). The 80/20 rise time of 2.1 ns is slower and the fall time of 2.9 ns is significantly faster compared to the values obtained for the more asymmetric pulse amplitudes of Fig. 4. Also a slight delay for the onset of switching becomes visible in Fig. 5(f). Saturation is reached before pulse reversal. At the falling edge vortices are formed again. However, the concertina is less pronounced in the top-down corners as compared to Fig. 4. Additional magnetization buckling develops in the left-right corner domains [Fig. 5(d)]. One additional detail becomes visible: For both, the rising and falling edge, small corner domains are apparent at the far left and right corners of the element [Figs. 5(a), 5(b), and 5(e)]. The direction of magnetization in these corners is obviously not switched due to the strongly reduced effective torque, caused by the large local demagnetizing field inside the corners. After reversing the field direction, the compressed edge-curling wall expands, forming the same small corner structures again.

The switching speed for different effective field amplitudes combining the 80/20 rise and fall times of the integrated change of magnetization [as shown in Figs. 4(k) and 5(f)] is given in Fig. 6. The switching occurs within several nanoseconds down to 0.6 ns for high field excitation. Only a small dependency on the field direction (i.e., rising and falling edge of the pulse) is found. This is rather unanticipated as the pulse shapes for the rising and falling edge differ strongly. The field amplitude is the dominating factor. Only in the low field regime [2 kA/m along the falling edge, Fig. 4(k)], where the gradual change of field with time at the falling edge is important, an additional reduction in switching speed is observed. At high fields (above 5 kA/m) no significant difference in switching velocity is measurable within our temporal resolution. From the discussion above it is valid to conclude that the field amplitude and the acting torque is the dominating factor influencing the speed of magnetization reversal. With the inhomogeneous field distribution in the element, depending on field characteristics, multiple domains involving vortices and domain boundaries are formed. Once domains are generated, the reversal is decelerated due to the low mobility of the domain-wall network.

For comparison we investigated a pointed element (Fig. 7). The applied field characteristic is the same as in Fig. 4. The element's shape is similar in character to the tilted square element investigated before, but not exhibiting the sharp left-right corners where the corner vortex structures appeared. Similar domain patterns during high field reversal along the rising edge of the field pulse are observed (compare Fig. 7 to Fig. 4), i.e., during switching antiparallel domains are formed. For the rising edge [Fig. 7(b)] a similar band domain structure as in Fig. 4(c) develops. Along the falling edge [Fig. 7(d)] the magnetization changes in the center region first. The sense of rotation is possibly imposed by a weak diagonally aligned uniaxial anisotropy, breaking the magnetic symmetry of the element (a tilted anisotropy was found from domain observation on extended elements on the same strip-line). Again, with the low driving field at the descending pulse, domains along the edges remain, annihilating slowly over some nanoseconds and still being present in Fig. 7(e). This becomes also visible in the quantitative analysis in Fig. 7, where no complete reversal is observed within the time-window of the measurement. For the pointed shape the local demagnetization field at the sides of the element is aligned parallel to the applied field axis. As a result a more homogeneous domain state without the opposing 90° domains (Fig. 4) develops. No pronounced vortex structure is formed. This confirms that the strong shape anisotropy in the corners is responsible for the development of the corner domains in the square shaped element, thus leading to the vortex structures. More dissimilarities in magnetization reversal can be observed in rectangular elements, as will be shown next.

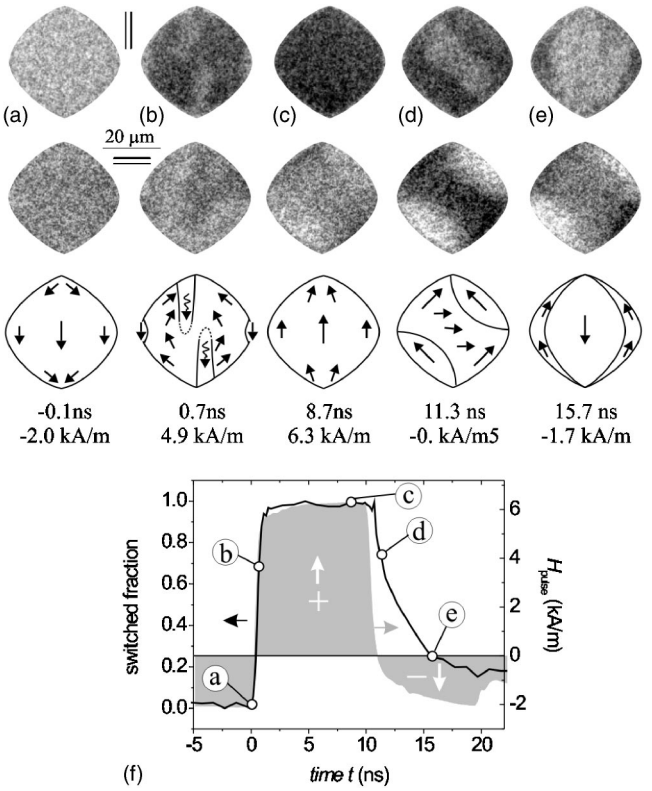

FIG. 7. Time-resolved Kerr images and domain interpretation of a pointed element. As in Fig. 4, the effective field varies from −2.0 to +6.3 kA/m. The relative position in time relative to the pulse onset and the effective field values are indicated. (f) Corresponding plots of the longitudinal Kerr signal along the field axis as a function of time.

The quasistatic magnetization reversal of a square element where the field is aligned parallel to the edges is displayed in Fig. 8. The main difference to the previously discussed case of diagonal field is that the switching begins primarily at the top and bottom edges [Fig. 8(b)], where the effective demagnetization field is highest. Starting from the edges a concertina pattern is formed, which then penetrates the element to the center region [Figs. 8(a)–8(c)]. In contrast to the tilted element, where the concertina period is rather small, the modulation period is larger due to the unrestricted width of the element [compare to Fig. 3(b)]. With reversed fields [Fig. 8(d)], the concertina collapses leaving a simple Landau ground state. With further increasing field amplitude the vortex moves towards the left edge.

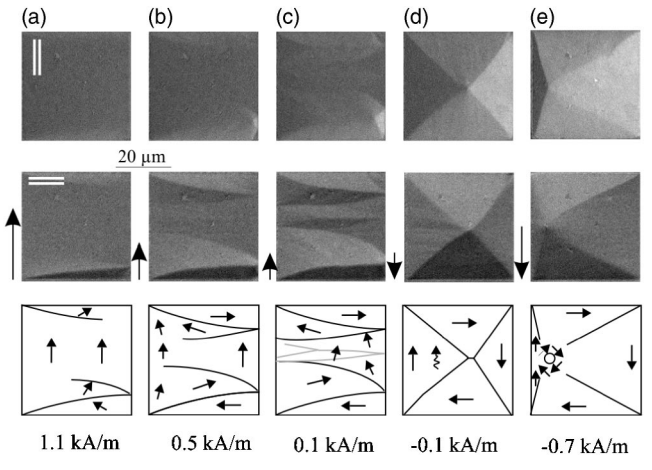

FIG. 8. Quasistatic magnetization process of a permalloy square in a magnetic field along the edge as indicated. Images are shown with the Kerr sensitivity longitudinal and transverse to the field axis. The schematic representation of the magnetization vector field is derived from the Kerr contrast.

The dynamic reversal process of this element, however, is not as clear. The domain development with fast changing field is shown in Fig. 9. The images were obtained under equal conditions as the pictures displayed in Figs. 4 and 7. With increasing field most of the magnetization reversal occurs within 1 ns [Figs. 9(a)–9(d)]. However, no distinct domain pattern becomes visible during reversal, neither for longitudinal nor transversal sensitivity. In contrast to the quasistatic case, the turnaround starts in the center of the element, which is best visible in the longitudinal image of Fig. 9(c). Only a weak modulation of magnetization becomes visible in the corresponding transversal image. In the longitudinal image of Fig. 9(d) the reversal seems to be already completed, but comparing the corresponding magneto-optical signal in Fig. 9(k) it becomes apparent that the element is not yet saturated. Residual domains at the edges are evident in the transversal images in Fig. 9(d), which annihilate after several nanoseconds [Fig. 9(e)]. The edge domains, however, are not sufficient in size to be responsible for the incomplete switching. Several other contributions may also contribute to the shown results. First our temporal resolution is limited to approximately 250 ps, which aggravates the visualization of fast changes well below 1 ns. In addition, the stroboscopic imaging technique relies on repeatable modes of magnetization reversal. This is not compelling in our case, where the center magnetization is more free to rotate and noconcertina patterns develop. Third, domains can be generated which are smaller in size than our lateral resolution. Furthermore, and connected to all arguments mentioned before, spin waves could be generated during reversal, which would not be detectable with the limited temporal and lateral resolution of our experiment.

The opposite low field reversal displayed in Figs. 9(f)–9(j) is very similar in character, but concertina domains develop in addition. Similar to the pronounced concertina of the tilted element (Fig. 4), the pattern resides during the change of magnetization [Figs. 9(g)–9(j)] as noticeable in the transversal images. The longitudinal edge domains generated are much more pronounced and vanish slowly. They are very similar to the edge domains shown before for the pointed element [Fig. 7(e)]. The whole reversal takes place over several nanoseconds [Fig. 9(k)]. Changing the bias field and thus equalizing the pulse fields for the rising and falling edges of the pulse, fast reversal for both pulse directions is achieved [Fig. 10(a)]. The remagnetization process occurs below 1 ns in both cases [Fig. 10(b)]. Further reversing the bias field and thus changing the effective pulse field does not display any additional changes in switching speed. The overall switching is much faster than for the tilted element [compare Fig. 10(b) to Fig. 6] due to the absence of the formation

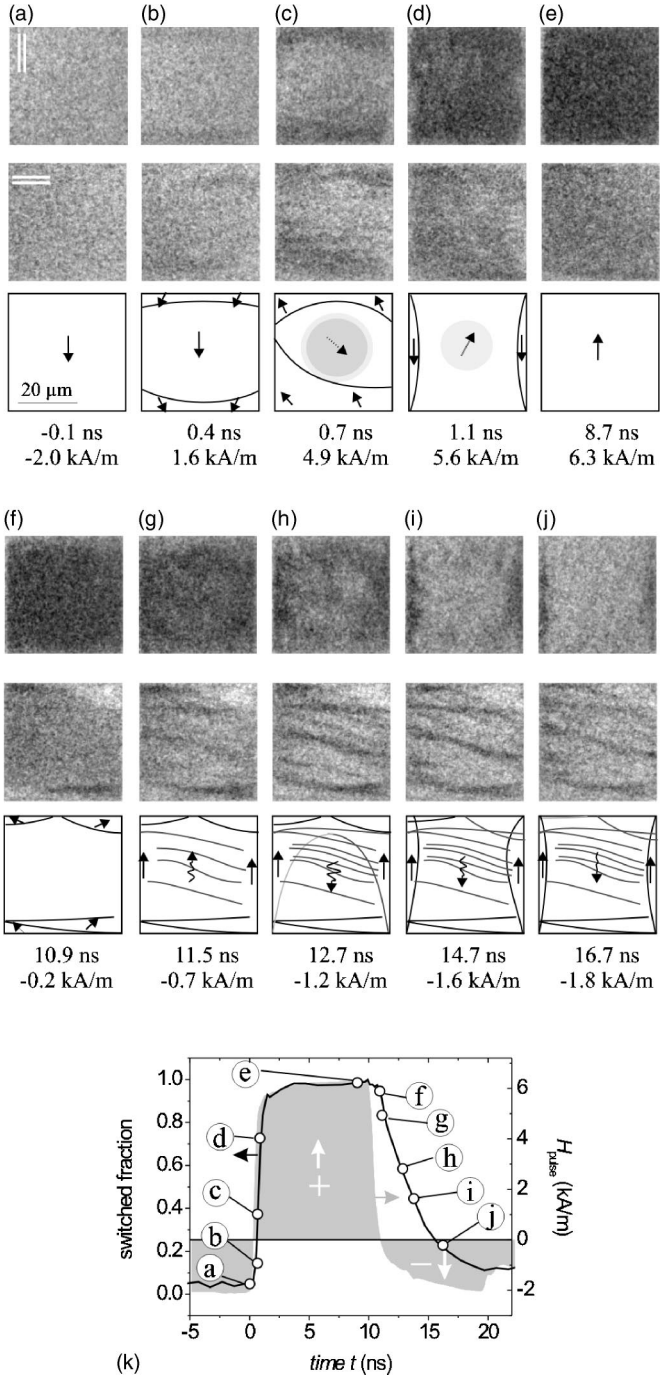

FIG. 9. (a)–(j) Time-resolved Kerr images at longitudinal and transverse sensitivity of the element shown in Fig. 8, but after excitation with a pulse field. Indicated is the effective field value and the time delay relative to the field pulse. In (c) no clear domain structure in the center of the element could be derived, as discussed in the text. (k) Plots of the longitudinal Kerr signal along the field axis as a function of time. The field varies from −2.0 to +6.3 kA/m.

of complicated domain states (except for the low field falling edge).

Reducing the elements width and thus increasing the shape anisotropy along the pulse field orientation slightly changes the characteristics, again. The quasistatic reversal of

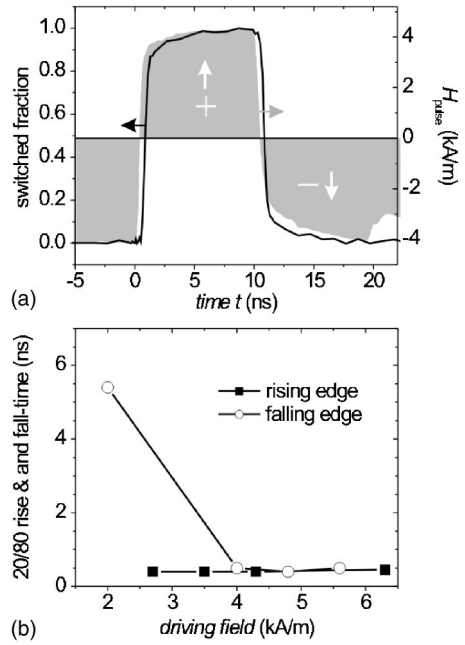

FIG. 10. Progression of the Kerr signal along the field axis as a function of time for the square element of Fig. 9. The field varies from −4.0 to +4.3 kA/m. (b) Rise and, respectively, fall times (from 20% to 80% of signal amplitude) for different driving pulse field amplitudes derived from the longitudinal response signal.

a rectangular element for almost the same field values as in the examples shown before is displayed in Fig. 11. The development of domains is very similar to the square element. Starting from saturation, a concertina pattern develops initiating from the top and bottom edges of the rectangular element [Figs. 11(a)–11(c)]. Nevertheless, one difference relative to the square element reversal becomes obvious. With the opposing field at −0.1 kA/m [Fig. 11(d)] the blocked domain state did not yet break down. Higher reversing fields are necessary to swap the magnetization in the narrower element. Moreover, the dynamic reversal displays differences to the process of the square element (compare Fig. 12 to Fig. 9). In contrast to the square element an indication for the rippled domain structures also exists along the rising edge [Fig. 12(b)]. The elongated element displays a striped domain pattern during field reversal, but more pronounced at the falling edge.

For a further increasing aspect ratio this trend is confirmed. The quasistatic images together with a domain inter-

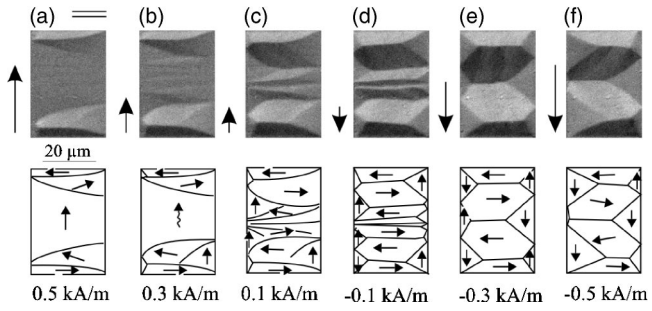

FIG. 11. Quasistatic magnetization reversal of a rectangular element (aspect ratio 3:2).

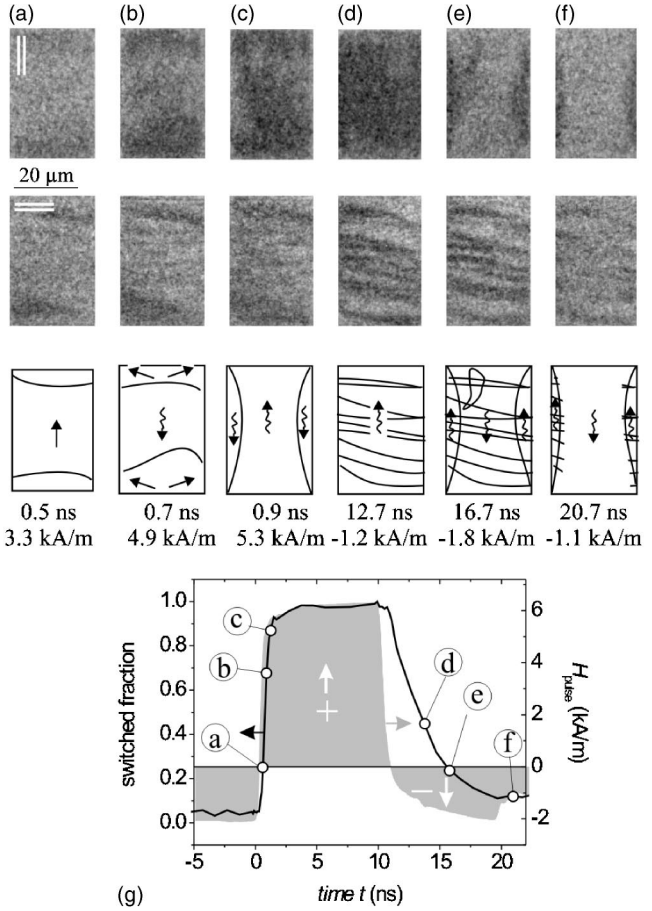

FIG. 12. (a)–(f) Dynamic Kerr images at longitudinal and transverse sensitivity of the element shown in Fig. 11. (g) Variation of the longitudinal Kerr signal as a function of time. The pulse field varies from −2.0 to +6.3 kA/m.

pretation for a narrow element of an aspect ratio of 4:1 are displayed in Fig. 13. Yet again, the domain formation starts from the top-down edges, moving into the element by concertina development [Figs. 13(a)–13(d)]. As for the other elements the initial process starts at the top and bottom edges by spike domain movement. A strictly rotational process, leading to the most narrow concertinas takes place in the center of the element. Still, with an opposing field of

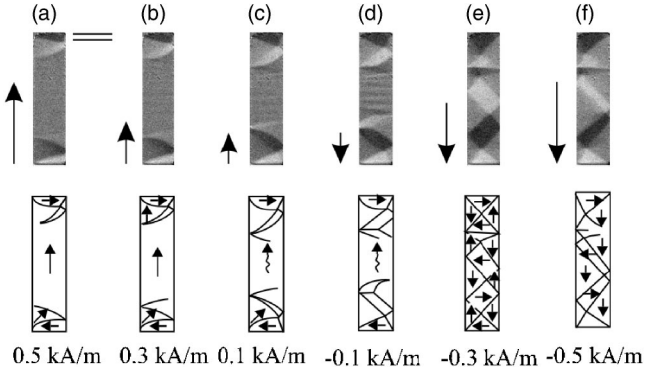

FIG. 13. Quasistatic magnetization reversal of a rectangular element (aspect ratio 4:1).

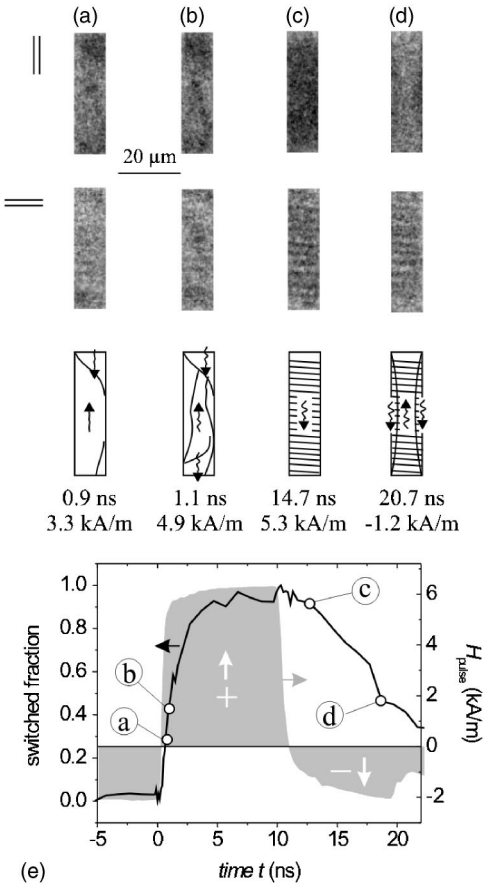

FIG. 14. (a)–(d) Dynamic Kerr images at longitudinal and transverse sensitivity of the element of Fig. 13. (e) Variation of the longitudinal Kerr signal as a function of time. The pulse field varies from −2.0 to +6.3 kA/m.

−0.1 kA/m [Fig. 13(d)] a narrow concertina pattern remains. As expected, the period of the concertina in the center portion of the element is much smaller than in the case of the wider elements.

The dynamic domains (Fig. 14) also display a pronounced preference for ripple domains. The magnetization process takes place by inhomogeneous magnetization rotation [Fig. 14(b)] along the rising edge. Also noticeable is that the blocked domain state occurs even close to saturation [Fig. 14(c)]. For smaller pulse amplitudes antiparallel aligned domains within the element occur and saturation is not achieved within the 10 ns pulse duration (not shown). Along the falling edge, a pronounced concertina pattern develops, the period of which is again much smaller than in the case of the wider elements. The frequency of the concertinas is very similar to the center part of the quasistatic remagnetization process. (Similar dependencies are also noticeable for the wider rectangular elements.) The initially striped character [Fig. 14(c)] remains even after partial longitudinal switching [Fig. 14(d)]. This is best visible from the nearly unchanged transversal sensitivity images. The residual domains along the edges annihilate over more than 10 ns. Domains along the edges where the magnetization is aligned antiparallel to the field hinder the remagnetization process [Fig. 14(d)], a slow change of magnetization in the element over a few

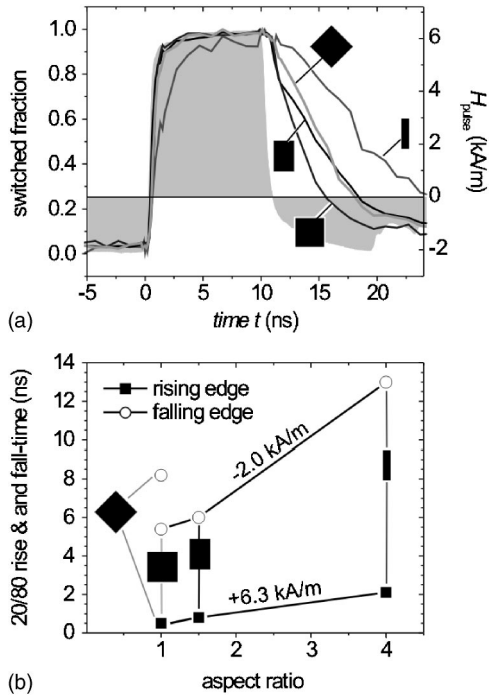

FIG. 15. (a) Evolution of the longitudinal Kerr signal along the field axis as a function of time for various element shapes. The wave form of the exciting pulse is shown. (b) Corresponding 80/20 rise and fall times for the curves shown in (a). The element shapes are sketched.

nanoseconds is observed [Fig. 14(e)]. Overall, the magnetization process in the narrow elements is slowed down drastically due to the development of narrow concertina structures.

A complete understanding of the described processes in the various elements can be gained by comparing the magnetic reversal in the differently shaped elements (Fig. 15). The dynamic magnetization reversal as shown in our experiments is determined by initial rotational processes, which lead to blocked domain states. The creation of blocking is preferential for narrower elements, where the magnetization cannot rotate as freely. The breakdown of the concertina, which in the quasistatic case occurs through domain wall reorganization, differs in the dynamic case, as the domain walls are much too slow to accommodate the remagnetization processes. The change of magnetization is slowed down by the generation of low angle domain walls or concertina-like patterns generated by magnetization rotation, a process sufficiently fast at the time scales investigated here. Congruently, we observe a decrease in switching time with decreasing width independent of field amplitudes for the rectangular $Ni_{81}Fe_{19}$ elements as seen from the time development of magnetization in Fig. 15(a) and the corresponding switching speed analysis in Fig. 15(b).

Another mechanism of deceleration is derived from our dynamic domain analysis. In addition and instead of a regular concertina breakdown, we in general observe the subsequent alteration of magnetization through the displacement of domain boundaries separating regions with nearly antiparallel magnetization. However, the existing blocked pattern

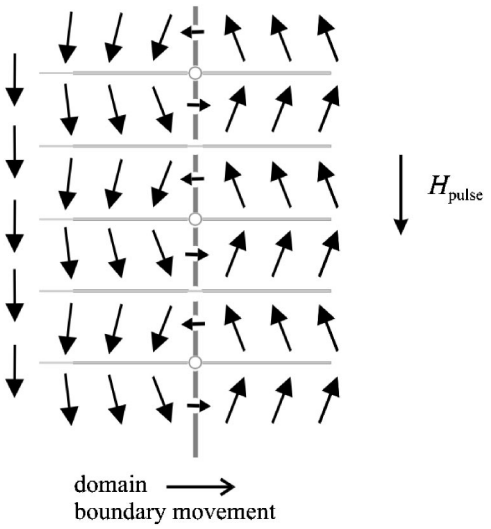

FIG. 16. Qualitative representation of the "cross-tie"-like domain boundary developing during high-speed reversal. Magnetic field and magnetization directions are indicated.

does not change its textured character around these domain walls after almost reversing the magnetization [e.g., compare Figs. 14(c) and 14(d) and the concertina structure in Fig. 4(j)]. Whereas the structure of the concertina or blocked domains remains visible in the transversal images, regions with up-down magnetizations form and change in time, which can be identified from the longitudinal images. For the tilted element, an even more complicated domain structure involving multiple vortices is formed, which leads to an even higher increase in switching time [see Fig. 15(b), aspect ratio $=1:1$] for the low field of -2.0 kA/m.

A likely structure of the domain boundaries in agreement with the various Kerr images is given in Fig. 16. Sketched is a blocked domain structure at the right side, which is separated from the already switched region, aligned parallel to the pulse field direction at the left side. As described above, whereas the magnetization is aligned up and down along both sides of the domain boundary, no change in the transversal magnetization component is observed. The domain boundary moves in accordance to the applied magnetic field. Noticeable is the similarity to the well-known cross-tie wall structure, which also consists of a chain of a different type of Bloch lines. However, the occurrence of these domain boundaries is related to the firstly developing concertina pattern and also differs strongly in period to cross-tie walls observed for $Ni_{81}Fe_{19}$ films of this thickness. The annihilation of the domain boundary network is strongly decelerated at the edges. This can be seen in almost all of our observations and also shows in the slow magnetic response for the small width elements, where the edge walls are contributing to a high degree to the overall magneto-optical signal.

IV. SUMMARY

In summary we investigated the domain formation in differently patterned $Ni_{81}Fe_{19}$ elements from dc to the nanosecond time scale. The development of the domains is strongly

determined by the shape and thus the penetrating field distribution during remagnetization. Depending on element shape and field amplitude, complicated domains with vortices and concertina form by magnetization rotation. The conversion of these patterns with the reversed field direction in the dynamic case happens through a mixture of rotation and domain boundary motion. The domain boundary evolves directly from the concertina pattern, resembling a cross-tie-like structure. However, the period of alternating Bloch lines is only determined by the early blocked domain state and not related to the much wider 90°-domain network cross-ties developing in extended NiFe films. Once complicated domains are generated the overall switching process is drastically slowed down due to the low mobility of vortex or Bloch lines together with the hindered annihilation of these structures at the element edges. Some of the results are believed to happen similarly in much smaller devices,[34] and have consequences for the understanding of switching events in polycrystalline thin film elements like MRAM devices.

ACKNOWLEDGMENTS

The authors thank O. deHaas (IFW Dresden) and R. Ahuja (LAVISION GmbH) for their valuable help in the conceptual stage of the stroboscopic setup. The film and stripline structures were fabricated in the department of C. M. Schneider (now FZ Jülich) at IFW-Dresden with the help of C. Krien and S. Sieber. The help of all colleagues is gratefully acknowledged. The work is supported by the Priority Program 1133 "Ultrafast magnetization processes" of the Deutsche Forschungsgemeinschaft.

*Electronic address: j.mccord@ifw-dresden.de
†Electronic address: r.schaefer@ifw-dresden.de

[1] A. Hubert and R. Schäfer, *Magnetic Domains—The Analysis of Magnetic Microstructures* (Springer-Verlag, Berlin, 1998).
[2] J. Miltat, G. Albuquerque, and A. Thiaville, *Spin Dynamics of Confined Magnetic Structures I* (Springer-Verlag, Berlin, 2002), pp. 1–33.
[3] T. Schrefl, J. Fidler, R. Dittrich, D. Suess, W. Scholz, V. Tsiantos, and H. Forster, *Spin Dynamics of Confined Magnetic Structures II* (Springer-Verlag, Berlin, 2003), pp. 1–26.
[4] R. Hertel and J. Kirschner, J. Magn. Magn. Mater. **270**, 364 (2004).
[5] R. L. Conger and G. H. Moore, J. Appl. Phys. **34**, 1213 (1963).
[6] W. Drechsel, Z. Phys. **164**, 324 (1961).
[7] B. Passon, Z. Angew. Phys. **25**, 56 (1968).
[8] G. Houze, J. Appl. Phys. **38**, 1089 (1967).
[9] L. Gal, G. Zimmer, and F. Humphrey, Phys. Status Solidi A **30**, 561 (1975).
[10] F. H. Liu, M. D. Schultz, and M. H. Kryder, IEEE Trans. Magn. **26**, 1340 (1990).
[11] B. Petek, P. Trouilloud, and B. Argyle, IEEE Trans. Magn. **26**, 1328 (1990).
[12] Y. Acremann, C. H. Back, M. Buess, O. Portmann, A. Vaterlaus, D. Pescia, and H. Melchior, Science **290**, 492 (2000).
[13] G. E. Ballentine, W. K. Hiebert, A. Stankiewicz, and M. R. Freeman, J. Appl. Phys. **87**, 6830 (2000).
[14] B. C. Choi, G. E. Ballentine, M. Belov, W. K. Hiebert, and M. R. Freeman, J. Appl. Phys. **89**, 7171 (2001).
[15] M. R. Freeman and W. K. Hiebert, *Spin Dynamics of Confined Magnetic Structures I* (Springer-Verlag, Berlin, 2002), pp. 93–126.
[16] W. Hiebert, L. Lagae, and J. De Boeck, Phys. Rev. B **68**, 020402 (2003).
[17] C. Back, R. Allensbach, W. Weber, S. Parkin, D. Weller, E. L. Garwin, and H. Siegmann, Science **285**, 867 (1999).
[18] J. Park, P. Eames, D. Engebretson, J. Berezovsky, and P. Crowell, Phys. Rev. B **67**, 020403 (2003).
[19] S.-B. Choe, Y. Acremann, A. Scholl, A. Bauer, A. Doran, J. Stöhr, and H. Padmore, Science **304**, 420 (2004).
[20] A. Krasyuk, A. Oelsner, S. Nepijko, A. Kuksov, C. Schneider, and G. Schönhense, Appl. Phys. A: Mater. Sci. Process. **76**, 863 (2003).
[21] J. Vogel, W. Kuch, M. Bonfim, J. Camarero, Y. Pennec, F. Offi, K. Fukumota, J. Kirschner, A. Fontaine, and S. Pizzini, Appl. Phys. Lett. **82**, 2299 (2003).
[22] A. Kuksov, C. Schneider, A. Oelsner, A. Krasyuk, D. Neeb, G. Schönhense, C. de Nadai, and N. Brookes, J. Appl. Phys. **95**, 6530 (2004).
[23] H. Stoll, A. Puzic, B. van Waeyenberge, P. Fischer, J. Raabe, M. Buess, T. Haug, R. Hoellinger, C. Back, D. Weiss *et al.*, Appl. Phys. Lett. **84**, 3328 (2004).
[24] A. Neudert, J. McCord, D. Chumakov, R. Schäfer, and L. Schultz (unpublished).
[25] *Camera system picostar hr 12*, URL www.lavision.de.
[26] H. van den Berg and D. K. Vatvani, IEEE Trans. Magn. **18**, 880 (1982).
[27] S. K. Decker and C. Tsang, IEEE Trans. Magn. **16**, 643 (1980).
[28] H. Hoffmann, IEEE Trans. Magn. **4**, 32 (1968).
[29] J. C. Slonczewski, B. Petek, and B. E. Argyle, IEEE Trans. Magn. **24**, 2045 (1988).
[30] A. deSimone, R. Kohn, S. Müller, F. Otto, and R. Schäfer, J. Magn. Magn. Mater. **242-245**, 1047 (2002).
[31] R. Schäfer and A. de Simone, IEEE Trans. Magn. **38**, 2391 (2002).
[32] R. Cantero-Álvarez and F. Otto, *Oscillatory Buckling Mode in Thin-Film Nucleation* (to be published).
[33] B. Choi, G. Arnup, M. Belov, and M. Freeman, J. Appl. Phys. **95**, 6540 (2004).
[34] A. Neudert (unpublished), micromagnetic simulations on submicron elements reveal similar domain pattern as in our experiments. For a tilted element also the formation of slowly annihilating edge vortices is found. However, no concertina patterns are formed.